Superconductor
Science and
Technology

PURPOSE-LED
PUBLISHING™

ACCEPTED MANUSCRIPT

Using high-temperature superconducting tapes to improve the generation of high-voltage pulses

To cite this article before publication: Thor Wens *et al* 2025 *Supercond. Sci. Technol.* in press https://doi.org/10.1088/1361-6668/ae0d0a

Using high-temperature superconducting tapes to improve the generation of high-voltage pulses

T. Wens[1], J.-F. Fagnard[1], C. Greffe[2], and P. Vanderbemden[1]

[1] University of Liege, Department of Electrical Engineering and Computer Science, B-4000 Liege, Belgium
[2] GeneriX SRL, B-4031 Angleur, Belgium

E-mail: twens@uliege.be

Abstract. This paper explores the integration of high-temperature superconducting tapes to improve the performance of Vector Inversion Generators (VIG), a family of compact and lightweight high-voltage pulse generators. In this work, our existing theoretical model of Vector Inversion Generators is updated to capture the impact of AC losses associated with superconducting tapes. Then, a first-ever experimental campaign on superconducting VIGs is conducted. The results confirm a voltage boost enabled by High-Temperature Superconducting (HTS) tapes, provided the substrate is non-ferromagnetic. Based on the validated model, the performance of VIGs with longer HTS tapes is projected, revealing that the boost in VIG performance achieved by reducing losses resulting from the use of superconducting material is more pronounced when the tape length is increased. Nevertheless, the use of superconducting tapes to improve the performance of VIGs is inherently limited in input voltage because of the non-linear behaviour of AC losses, which can cause the losses associated with HTS tapes to become higher than the ohmic losses of copper tapes. As a consequence, to improve the performance of VIGs for increased values of input voltage, one can either use HTS tapes with higher critical currents, use methods to reduce AC losses - such as filamentisation or striation of coated conductors -, or investigate other methods to enhance VIG performances, such as lower inductance switch designs.

Vector Inversion Generators, Pulsed power, Voltage multiplication, High-temperature superconductors

1. Introduction

Generating high-voltage pulses ranging from a few kilovolts to several hundreds of kilovolts is of interest in a wide range of industrial applications, such as rock fracturing [1] or food sterilisation [2]. Several topologies exist to generate such pulses, such as Marx generators [3], Tesla transformers [4], or Vector Inversion Generators (VIGs) [5], which are the kind of generators studied in this work. This topology of pulse generators is well-known for its compactness. Basically, a Vector Inversion Generator consists of a capacitor (two conducting layers) wound as a spiral of N turns. Each conducting layer is separated from the neighbouring ones by dielectric layers. A single switch, hereafter called the "input switch", connects the two conducting layers at the input of the spiral. A schematic view of such a pulse generator is shown in Figure 1.

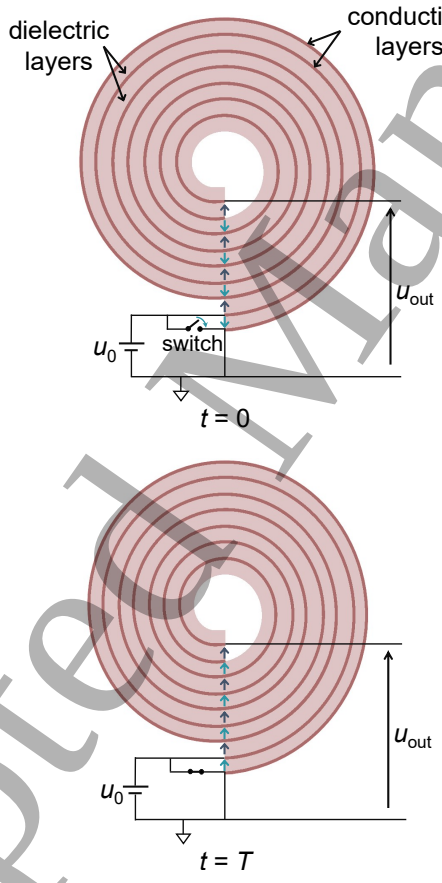

Figure 1. Schematic view of the working principle of Vector Inversion Generators.

Prior to the generation of the output high-voltage pulse, the capacitor is fully charged with a DC voltage u_0. As a consequence, the electric field vectors of adjacent turns point towards opposite directions, resulting in a zero output voltage. At $t = 0$, the input switch closes, causing an electromagnetic wave to propagate inside the spiral. This electromagnetic wave is reflected at the inner open extremity of the spiral. It

takes a period T for the wave to travel back and forth inside the spiral. So, at $t = T$, the wave returns to the location of the switch and all electric field vectors are aligned, and the output voltage reaches, in theory, $-2Nu_0$ [6]. The electromagnetic wave is then reflected at the outer extremity of the spiral (i.e., at the location of the switch) and continues to travel back and forth in the spiral, resulting in a triangular output voltage that should oscillate between $u_{\text{out}} = 0$ and $u_{\text{out}} = -2Nu_0$, as illustrated in the green curve of figure 2 which provides typical schematics of the ideal and real input and output voltage waveforms. In practice, there are several non-idealities, such as the finite fall time of the switch, ohmic losses, or undesired secondary wave propagations, which cause the output waveform to not be triangular. The output voltage actually oscillates between extrema of different peak amplitudes that are lower than $2Nu_0$, as illustrated by the red curve of figure 2. In some cases, the amplitude of the second peak exceeds that of the first one [7, 8], but the following peaks are usually smaller than the first two. Therefore, the first two peaks are those of interest in practice. To take into account the non-idealities of the generator, two voltage division efficiencies $\beta_1 \leq 1$ and $\beta_2 \leq 1$ are introduced such that the amplitudes of the two first first peaks are expressed as $u_{\text{out},1} = -2N\beta_1 u_0$ and $u_{\text{out},2} = 2N\beta_2 u_0$. The output voltage can also be expressed by introducing two voltage multiplication coefficients K_1 and K_2 such that $u_{\text{out},1} = -K_1 u_0$ and $u_{\text{out},2} = K_2 u_0$.

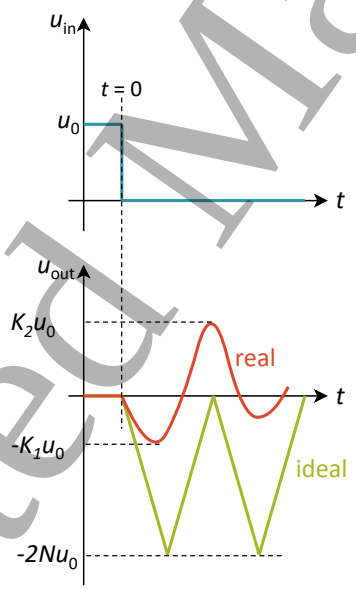

Figure 2. Schematic view of typical ideal and real output voltage waveforms.

Several factors affect the voltage multiplication efficiency β [9], one of them being resistive losses in the conductors as the electromagnetic wave travels the spiral. This factor is responsible for a reduction of about 10% of the voltage multiplication efficiency. For this reason, it is of interest to replace copper that is traditionally used for winding vector inversion generators with high-temperature superconducting (HTS) coated conductors tapes in view of increasing the voltage multiplication efficiencies.

HTS coated conductors are already commonly used to replace copper in wide range of applications, such as energy and transport [10, 11], magnetic energy storage [12, 13], rotating machines [14–16], current transport [17, 18], high-field magnets [19–21], or thermonuclear fusion reactors [22].

The goal of this paper is to explore how to improve the performance of Vector Inversion Generators (VIG) by using high-temperature superconducting tapes. To do so, our previously established semi-analytical model of VIGs [7] is updated to account for AC losses of HTS tapes. It is then confronted with experimental data to validate that it can be used to predict the benefits of using HTS tapes for VIGs with larger geometries. These measurements also enable a direct comparison between VIGs wound with HTS tapes and an equivalent copper-wound design, confirming the performance gains offered by superconducting configurations. Additionally, prototypes with and without a ferromagnetic substrate are tested to evaluate how substrate properties influence the output voltage.

2. Theory

2.1. Replacing Cu by HTS with AC-losses

In our previous work [7], we have established an updated transfer function allowing one to predict analytically the Laplace transform of the output voltage of Vector Inversion Generators based on a set of dimensionless parameters. Appendix A provides a brief explanation of our model as well as the complete set of dimensionless parameters. Among this set of parameters used in the analytical model, two account for losses in the conductive layers. The first one, denoted ρ_0 is used to express the losses of the two waveguides formed by the conductors wound as a spiral. The active waveguide consists of the main spiral capacitor, i.e. two conducting layers separated by a dielectric layer that are connected to the input switch, whereas the passive waveguide consists of the conducting layers separated by the dielectric layer used to insulate the turns of the capacitor wound as a spiral. The second parameter, ρ_p is used to account for the resistance of the outer turn of the spiral as well as the non-zero resistance of the input switch. The two dimensionless parameters accounting for the losses in the generator are expressed as:

$$\rho_0 = \frac{R'T}{L'} \quad \text{and} \quad \rho_p = \frac{R_s + R_{turn}}{Z_0} = \frac{R_s + R'\pi D_{out}}{Z_0}, \tag{1}$$

where R', L', and C' are respectively the resistance, inductance, and capacitance per unit length of the waveguides, R_s is the resistance of the input switch, and $Z_0 = (L'/C')^{1/2}$ is the characteristic impedance of the waveguides, assumed to be identical for both active and passive waveguides. The parameter T is the time required for the electromagnetic wave to travel back and forth in the spiral. R_{turn} is the resistance of the outer turn of the spiral, and can be expressed as $R_{turn} = R'\pi D_{out}$, with D_{out} the diameter of the outer turn of the spiral. In this work, R' is the parameter of interest as it is directly linked to the conductivity σ of the material, which is the physical parameter that will vary according to the nature of the conducting tape. For an ohmic (i.e. linear) conducting layer, R' is dictated by the skin effect:

$$R' = (\sigma h \delta)^{-1}, \tag{2}$$

where h is the width of the conducting layers, and $\delta = (\pi f \sigma \mu_0)^{-\frac{1}{2}}$ is the skin depth which is a function of σ, the frequency f, and the magnetic permeability μ_0 of the conducting layer, which is supposed to be non-magnetic. Replacing with the expression of δ, one obtains:

$$R' = \frac{\sqrt{\pi}}{h}\sqrt{\frac{\mu_0 f}{\sigma}}. \tag{3}$$

Contrary to ohmic conducting layers, HTS tapes exhibit non-linear lossy behaviour, meaning that the losses directly depend on the current flowing in the tape. As the model used in this paper to predict the output voltage of VIGs is linear, the model can be used provided that the current I that will flow inside the HTS tapes can be approximated. The resistance per unit length R' is then given by:

$$R' = \frac{P'}{I^2}, \tag{4}$$

where P' is the losses per unit length in the HTS tapes. This quantity can be estimated using the Norris relation for losses in HTS tapes with a rectangular cross section [23]:

$$P' = \frac{\mu_0 f I_c^2}{\pi}\left[(1-i)\ln(1-i) + (1+i)\ln(1+i) - i^2\right], \tag{5}$$

in which $i = I/I_c$, with I_c the critical current, ranging from hundreds to thousands of amperes for the HTS tapes used in this work, as will be explained in section 3. Using Eq. 5, the resistance per unit length R' used for HTS tapes given by equation 4 rewrites as:

$$R' = \frac{\mu_0 f}{\pi}\,\frac{(1-i)\ln(1-i) + (1+i)\ln(1+i) - i^2}{i^2}. \tag{6}$$

Including this frequency dependant expression of R' in the Laplace domain was performed following the procedure presented in [24], in which transient losses in transmission lines are studied. The remaining step to estimate losses in the waveguide is to find a value for the current I. When the capacitor connected to the input switch is charged initially with a DC voltage u_0, a very good approximation for the current flowing in the waveguides is given by $I = \frac{u_0}{Z_0}$ [25]. The characteristic impedance of the waveguides Z_0 can be calculated from their geometric characteristics and the permittivity of the dielectric layer. The order of magnitude of this characteristic impedance of a VIG is about a few ohms, corresponding to currents in the order of hundreds of amperes.

2.2. Magnetic diffusion towards the superconducting layer

In conventional VIGs, the conductors of the waveguide consist of copper directly in contact with the dielectric layer. In the superconducting VIGs investigated in this work, one important difference is that the superconducting layer of a coated conductor is only a small portion of the cross-sectional view of the conductor and is sandwiched between normal conductors [26]. Some coated conductors, such as the ones that will be used in the experimental part of this work, contain a copper stabilising layer on each side. Currents appear in the conducting layers because of the varying magnetic field in the dielectric medium of the waveguides. As a consequence, the currents therefore first establish at the outside extremities of the tape, and only flows in the superconducting layer once the magnetic field has diffused towards the superconducting layer. This

paper concerns generators of pulses having a rise time in the order of tens to hundreds of nanoseconds, which are characteristic times comparable to the time constants of magnetic diffusion inside the normal conductors of the tape. So, when using coated conductors to wind a vector inversion generator, an important question that arises is whether there is enough time for the current to establish in the superconducting layer before the pulse is fully erected. To answer this question, the time needed by the magnetic field to diffuse in the normal conductor should be estimated by solving the 1D magnetic diffusion equation as follows [27]:

$$\begin{cases} \dfrac{\partial H}{\partial r} - \dfrac{1}{\sigma\mu_0}\dfrac{\partial^2 H}{\partial r^2} = 0, \\ J = \dfrac{\partial H}{\partial r}, \end{cases} \tag{7}$$

where H is the magnetic field, J the current density, and $z = 0$ is the interface between the dielectric medium and the HTS tape, as shown in figure 3. The magnetic diffusion equation is established by combining the Maxwell equations with the constitutive law $J = \sigma E$. The displacement current can be dropped in the Ampere-Maxwell law because the problem is solved only for the conducting layer, which is still in the conducting region for the time scales of interest [28]. The conducting layer is supposed to be non magnetic, hence the use of μ_0 for the magnetic permeability.

The characteristic time associated with the magnetic diffusion over a characteristic length ℓ_c is given by $\tau_d = \sigma\mu_0\ell_c^2$. In liquid nitrogen, copper has a conductivity of about $7.4{\cdot}10^8$ S/m [29], which is about two orders of magnitude higher than that of Hastelloy, which is about $8.3{\cdot}10^6$ S/m [30]. The thickness of the copper stabilising layer can range from a few microns up to about 100 µm [31,32] while the thickness of the substrate is usually between 50 µm and 100 µm [33]. This corresponds to characteristic diffusion times in the range of hundreds of nanoseconds for copper, compared to tens of nanoseconds for the substrate layer. For this reason, it is assumed that the most critical part of the magnetic diffusion is in the copper stabilising layer, and the magnetic diffusion problem given by equation 7 is solved for copper only. Figure 3 shows a schematic illustration of the problem that is solved: a magnetic field stimulus $H_{\mathrm{app}}(t)$ associated with the wave propagating in the spiral is applied at the boundary between the dielectric material and the copper layer, at $r = 0$. This stimulus generates a magnetic field $H(r,t)$ and a current density $J(r,t)$ which diffuses in the conducting layer in the r direction.

The input stimulus $H_{\mathrm{app}}(t)$ is assumed to follow an exponential rise, with a characteristic time τ_s corresponding to the fall time of the input switch, which is typically 10 ns:

$$H_{\mathrm{app}}(t) = H_0\left(1 - e^{-t/\tau_s}\right) \tag{8}$$

The diffusion problem consists of solving the set of equations 7 using equation 8 as a boundary condition. Figure 4 shows the results of the diffusion problem over a time range of 150 ns and for different depths r inside the copper layer. Figure 4a is a plot of the normalised magnetic field $H(r,t)/H_0$ for different times ranging from 10 ns to 150 ns. Figure 4b contains a similar set of curves for the normalised current density $J(r,t)/J_0$, where J_0 is defined as H_0/δ^* where δ^* is a characteristic length defined as $\delta^* = [\tau_s/(\sigma\mu_0)]^{1/2}$. Considering an arbitrary threshold of $J(r,t)/J_0$ of

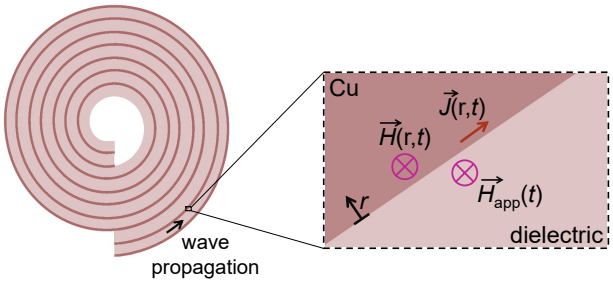

Figure 3. Schematic view of the magnetic diffusion problem at the boundary between the dielectric layer and the copper layer of the HTS tape. The applied stimulus is H_{app} and the computed variables are $H(r,t)$ and $J(r,t)$.

10^{-4} as a criterion for which the current density is high enough to be considered non-negligible, it can be seen in the graph that less than 20 ns are required for the current to establish over copper widths below 25 µm. For a copper width of 50 µm, about 85 ns are required for the current to diffuse, and for a copper width of 70 µm, it takes more than 150 ns for the current to establish. The results of the magnetic diffusion problem show that for HTS tapes having a copper stabilising layer, a certain amount of time, referred to as T_{diff} in the remainder of the discussion, is required before the current flows in the superconducting region. For a VIG with HTS tapes to be efficient, it is important that the current can reach the superconducting layer of the HTS tape in the entire spiral before the vector inversion process terminates. For this reason, T_{diff} must be much smaller than the time T required for the wave to travel back and forth inside the spiral. This can be expressed mathematically as:

$$T \gg T_{\mathrm{diff}} \Leftrightarrow \frac{2N\pi D_{\mathrm{mean}}}{c/\sqrt{\varepsilon_{\mathrm{r}}}} \gg T_{\mathrm{diff}}, \tag{9}$$

where D_{mean} is the mean diameter of the spiral, c the speed of light in free space and ε_{r} the relative permittivity of the dielectric layer. Taking into account the small but finite thickness of the stabilising layer, the practical conclusion to be drawn from the above study is that a minimum length of coated conductor is needed for the HTS tapes to be of interest for the conducting layers of a VIG, and this minimum length increases strongly with the thickness of the copper stabilising layer. For example, considering a VIG wound with a mean diameter D_{mean} of 50 mm, one can find that N must be respectively $N \gg 2$, $N \gg 11$, and $N \gg 43$ for copper stabilising layers of 10, 25, and 50 µm. These results were obtained by solving equation 9 for values of T_{diff} found via the magnetic diffusion problem introduced in the set of equations 7. The value $\varepsilon_{\mathrm{r}} = 3.4$ was used, considering polyimide as dielectric medium, as will be used in the experimental part of this work.

3. Experimental methods

To evaluate experimentally the benefits of using HTS tapes in Vector Inversion Generators, several prototypes are built, each with the same inner diameter $D_{\mathrm{in}} =$ 50 mm and number of turns $N = 20$. All prototypes use Kapton® for the dielectric medium between conducting layers. Their main differences are summarized in Table 1. The first prototype, referred to as SC-6-NF, is wound with a 6-mm-wide coated

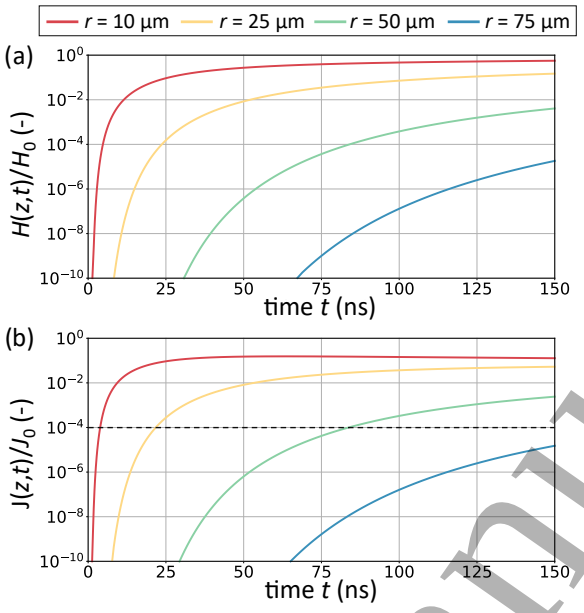

Figure 4. Solution of the magnetic diffusion problem for copper for different depths of copper. (a) Normalised magnetic field $H(r,t)/H_0$. (b) Normalised current density $J(r,t)/J_0$.

conductor from the TPL4000 series from *Theva GmbH*). The substrate is non-magnetic (Hastelloy® C-276), 50 µm-thick, and the average self-field critical current at 77 K provided by the manufacturer is 340±20 A. The second superconducting prototype, named SC-40-F, uses 40-mm-wide coated conductor N4311856 by *Deutsche Nanoschicht GmbH*. The substrate (Ni5W) is ferromagnetic, and the average self-field critical current at 77 K specified by the manufacturer is 1350±67 A. For reference, two copper-based VIGs are also wound: Cu-6, for comparison with SC-6-NF, and Cu-40, serving as the benchmark for SC-40-F.

VIG	height h	total tape thickness	Cu layer ?	magnetic substrate ?
SC-6-NF	6 mm	60 µm	✓	✗
Cu-6	6 mm	50 µm		
SC-40-F	40 mm	65 µm	✗	✓
Cu-40	40 mm	50 µm		

Table 1. Comparison between the different VIG that were wound to experimentally compare VIGs with copper tapes with VIGs with HTS tapes.

Figure 5 is a photograph of the experimental setup used for the measurement of the output voltage. The tested VIG is placed inside a polystyrene container that can be filled with liquid nitrogen. The input switch consists of a Gas Discharge Tube (GDT), which self-triggers at a given threshold voltage that depends on the nature of the gas. Several GDTs are used to cover a wide range of input voltages, namely the 2049 series from *Bourns*® for voltages below 300 V, or model A71H10X from *TDK Electronics* for a trigger voltage of 1 kV. It should be noted that, while it is not

explicitly mentioned in the datasheets, the experimental tests performed in this work also showed that GDTs are able to operate in liquid nitrogen with almost no variation of trigger voltage. It should also be noted that the DC input voltage is applied across the Kapton® layer between two superconducting tapes, which differs from the geometry used for electrical breakdown tests using coated conductors [34, 35]. The input voltage is monitored using a CT4079 differential probe from *Elditest*, and the output voltage is measured using a P6015A probe from *Tektronix*®. The probe outputs are connected to a TDS2204B oscilloscope from *Tektronix*®.

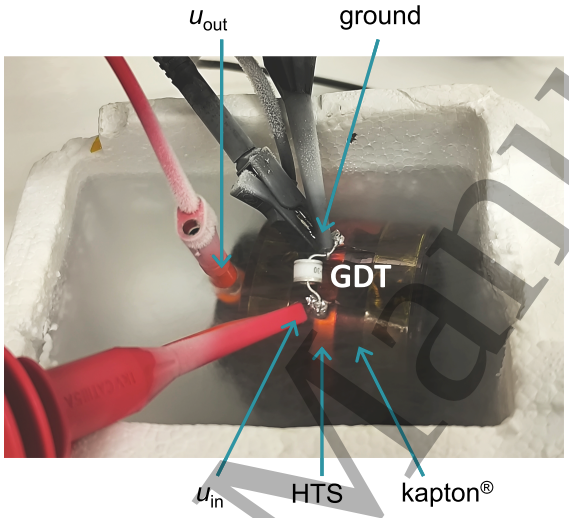

Figure 5. Photograph of the experimental setup.

4. Results and discussion

4.1. Experimental results

This section provides the experimental results associated with the measurements of the output voltage of the VIGs presented in Section 3. First, in Section 4.1.1, the measurement of the output voltage of SC-6-NF in liquid nitrogen is compared with a prediction of our semi-analytical model to validate it. Second, in Section 4.1.2, each VIG wound with HTS tapes is compared to its reference copper VIG, both at room temperature (293 K) and at cryogenic temperature (77 K).

4.1.1. Model validation: This section aims at providing an experimental validation of the way our model has been updated to account for AC losses in HTS tapes. Figure 6 shows a comparison between the dimensionless output voltage u_{out}/u_0 predicted by the updated version of our previously established model and a measurement carried out in liquid nitrogen using the superconducting VIG SC-6-NF. As can be seen in the figure, there is a good agreement between the experimental data and the prediction of the model, especially for the first two peaks, which are usually the ones used to characterise VIG behaviours. As a matter of fact, in engineering applications, VIGs

are often connected to highly non-linear loads such as X-ray tubes [36], causing the output voltage waveform to return to zero typically after the first or the second peak. That is the reason why the discrepancy that can be observed in figure 6 for the third peak of the output voltage has usually no consequence in practical applications in which the VIG is connected to a non-linear load. The first peak appears to be somewhat underestimated, and the model slightly underestimates the period of the output oscillations and begins to slowly diverge after the first two peaks. This slight underestimation of the oscillation period was also observed for non-superconducting VIGs, as shown in [7] when the results of the model are compared to experimental output voltage results using VIGS made with copper tapes. The small oscillations that are visible in the experimental trace are attributed to noise picked up during the measurement and are not related to the physics of vector inversion generators. The results plotted in figure 6 provide an experimental validation of the way we model VIG with superconducting materials.

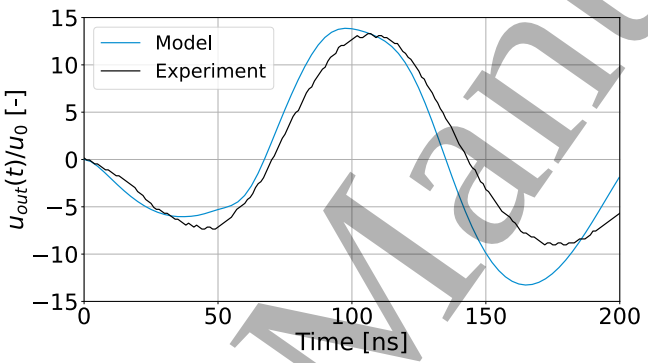

Figure 6. Comparison between the prediction of the model and an experimental waveform for VIG SC-6-NF at cryogenic temperature.

4.1.2. Comparison with copper VIGs This section presents the experimental performance of VIGs wound with HTS tapes, both with and without ferromagnetic substrates. The analysis compares these devices with their respective copper reference VIGs, focusing on the voltage amplitudes of the first two peaks of the output voltage at both room temperature (293 K) and cryogenic temperature (77 K). The comparison is expressed using the values of the multiplication coefficients K_1 and K_2.

Figure 7 shows histograms of the values of K_1 and K_2. Figure 7a shows the results for the VIG wound with an HTS tape without ferromagnetic substrate (SC-6-NF) compared to the copper reference Cu-6, and figure 7b contains the results for the VIG wound with an HTS tape containing a ferromagnetic substrate (SC-40-F) compared to the copper reference Cu-40.

Focusing first on figure 7a, it can first be seen that, at room temperature (red histograms), the multiplication coefficients of VIGs wound with HTS tapes are slightly lower than the reference VIG with copper. This result is particularly visible for the multiplication coefficient of the second peak K_2. This is most likely explained by the fact that, at room temperature, the current of the VIG SC-6-NF flows through the

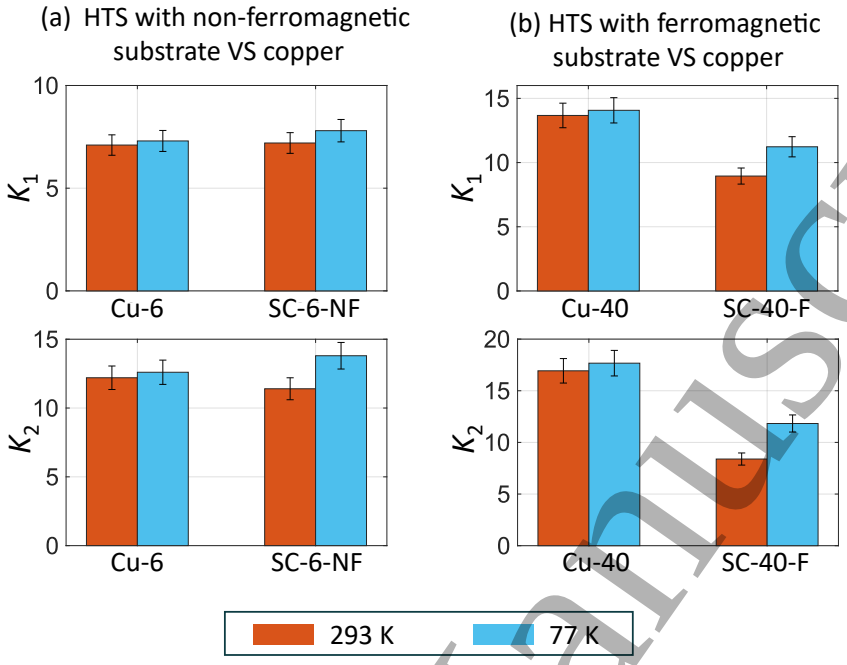

Figure 7. Histograms of the experimental values of the multiplication coefficients of the first two peaks of u_{out} for all the prototypes at both room and cryogenic temperatures. (a) Non ferromagnetic substrate. (b) Ferromagnetic substrate.

substrate and the copper stabilising layer. At room temperature, the substrate has a conductivity that is about one order of magnitude below that of copper, and the copper stabilising layer has a thickness of 10 µm, while the copper tape used for the VIG Cu-6 has a thickness of 50 µm. This results in a higher electrical resistance of the waveguides for the VIG SC-6-NF compared to the VIG Cu-6, and, as a direct consequence, a lower multiplication coefficient. This observation is not entirely consistent with the value of K_1, for which the values are almost identical for the reference VIG and the VIG wound with HTS tape. This can be explained by a manufacturing error during the winding, causing slight geometrical differences between the prototypes. As the first peak is less affected by ohmic losses, the effect of the small geometric differences between the VIGs probably outweighs the impact of the small difference in electrical resistances of the conductors at room temperature. Second, it can be observed that, at cryogenic temperature, both VIGs made of Cu and HTS tapes exhibit higher values of K_1 and K_2 than at room temperature, but SC-6-NF exhibits better multiplication coefficients than its reference copper VIG. This result was expected as, at cryogenic temperature, the current mainly flows through the superconducting layer of the HTS tape once the diffusion process is established. This results in reduced losses and, therefore, increased multiplication coefficients. The boost of K_2 is more significant than the boost of K_1. This observation can probably be explained by the magnetic diffusion inside the conducting tapes, according to the results found in the theory section. The tapes used to wind SC-6-NF have a 10 µm copper stabilising layer. It was shown in Section 2.2 that $N \gg 2$ is required, considering that a factor $\times 10$ is

required, $N = 20$ should be sufficient. But it must be remembered that the underlying assumption when establishing the magnetic diffusion theory was that the diffusion only occurs in the copper layer. Nevertheless, for this thickness of copper, which is the smallest of the ones studied in the theory section, the characteristic magnetic diffusion time inside the copper stabilising layer is 93 ns the characteristic magnetic diffusion time inside the substrate layer is 26 ns. While the characteristic time associated with the substrate layer is indeed smaller, it is not negligible compared to the characteristic time associated with that thickness of copper. This means that a non-negligible fraction of T is required for the current to fully establish in the superconducting layer, but the current is fully established in the superconducting layer for the second peak.

The behaviour of the VIG wound with HTS tapes containing a ferromagnetic substrate (SC-40-F) is now considered. As can be observed in figure 7b, the copper reference VIG Cu-40 exhibits better voltage multiplication coefficients than the superconducting VIG SC-40-F, even at cryogenic temperature. The performance degradation of the superconducting VIG is attributed to magnetic losses introduced by the ferromagnetic substrate: while ohmic losses are reduced through the use of HTS tapes, the additional magnetic losses outweigh these benefits. This is even more visible in figure 8, in which oscilloscope traces of the time evolution of the output voltages are plotted for VIGs SC-6-NF and SC-40-F. These measurement data were obtained in liquid nitrogen when using GDTs with a nominal trigger voltage of 1 kV. It can be observed that the output voltage oscillations are slowly damped, and there are still some remaining oscillations 1 µs after the closing of the switch. On the contrary, for the VIG with a ferromagnetic substrate, the output voltage oscillations are almost immediately damped, giving evidence that there are additional losses.

4.2. Model prediction for higher numbers of turns

As the comparison with experimental data showed that the updated model is suitable for predicting the behaviour of superconducting VIGs, it is now possible to predict the benefit of using HTS tapes to wind VIGs with increasing lengths of tapes, *i.e.*, by increasing the inner diameter D_{in} or the number of turns N. To do so, our model is used to predict the multiplication coefficient K_1 of the first peak of the output voltage when the number of turns varies from $N = 25$ to $N = 200$ for a VIG with an inner diameter $D_{\mathrm{in}} = 150$ mm. As the only source of losses considered in the model are AC losses, this study assumes that the HTS tapes contain a substrate that is not ferromagnetic. Such a study was not performed for the second voltage peak, associated with K_2, because this second peak arises from the complex interaction of different mechanisms and LC resonances [37], causing constructive or destructive interferences. This leads to highly variable waveforms that preclude systematic analysis, unlike the first peak K_1, which exhibits clear, monotonic behaviour with increasing number of turns. In the theory of Vector Inversion Generators, it is known that the value of the inductance of the input switch L_{s} plays a major role in the amplitude of the output voltage [8, 9]. For this reason, the predictions are provided for two different values of the inductance of the switch: $L_{\mathrm{s}} = 10$ nH and $L_{\mathrm{s}} = 50$ nH. The results are plotted in figure 9. Several curves are plotted in this figure. The dashed black lines correspond to the ideal case, where the conducting tapes exhibit no loss at all. The two curves with square markers represent the results for copper: the red markers correspond to the data at room temperature (293 K), and the pink markers at cryogenic tempera-

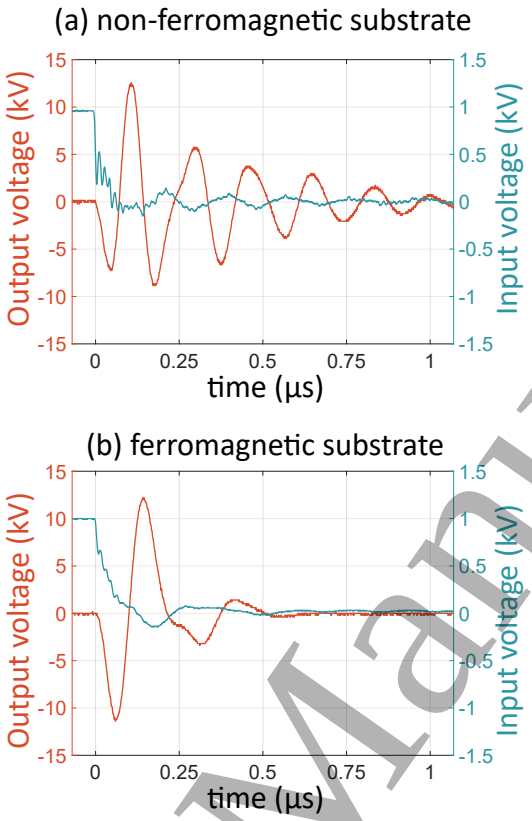

Figure 8. Experimental waveforms of the input and output voltages of Vector Inversion Generators at cryogenic temperature. (a) Without magnetic substrate. (b) With ferromagnetic substrate.

ture (77 K). Finally, the blue curves with round markers represent the results for HTS tapes at 77 K for several values of the ratio $i = I_{\max}/I_c$.

A first global observation that can be done is that all the values of K_1 of figure 9b exceed the values of their equivalent curves of figure 9a. This shows that, while this paper mainly focuses on the benefits obtained by reducing ohmic losses, parameters related to other parts of the VIG (here, the switch) also have an influence on VIG performances.

A second global observation is that the voltage multiplication coefficient increases when the number of turns increases, but not in a linear fashion. As the multiplication coefficient of the first peak is expressed as $K_1 = 2N\beta_1$, the curvature of $K_1(N)$ shows that β_1 decreases as N increases. In both figures 9a and 9b, the gap between the black curve (no loss) and the red curve (copper at 293 K) increases as N increases, showing that the reduction of β_1 caused by ohmic losses increases as N increases. The practical conclusion to take from this observation is that the benefits of investigating superconducting VIGs are more pronounced when the number of turns increases.

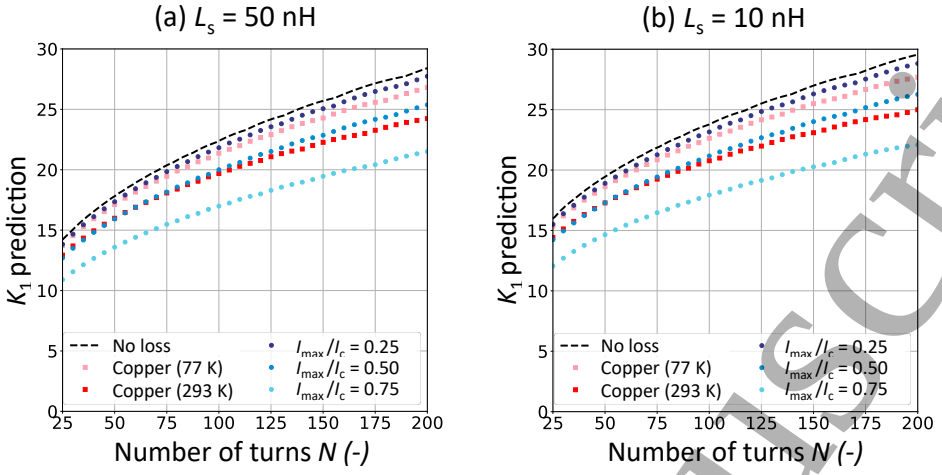

Figure 9. Model predictions for the multiplication coefficient K_1 of the first peak of u_{out} with an VIG diameter of 150 mm and two values of the input switch inductance. As the model only accounts for AC losses, HTS tapes without ferromagnetic substrates are considered here. Each configuration is investigated for different scenarios of the ohmic losses: lossless tapes (ideal case), copper tapes at 293 K, copper tapes at 77 K, and HTS tapes with different values of the current ratio $i = I_{\text{max}}/I_{\text{c}}$.

A third important observation is that VIGs with HTS tapes suffer from a limitation caused by AC losses of superconducting tapes. It can be seen in the different sets of curves that the ratio $i = I_{\text{max}}/I_{\text{c}}$ sets the limits of the improvement of VIG performances when using HTS tapes. To outperform the results of copper at 77 K, the value of i should be kept below 0.25. As a VIG consists of waveguides, the value of I_{max} can be estimated as u_0/Z_0, where Z_0 is the characteristic impedance of the waveguides constituting the spiral. For a VIG with a given geometry, this sets the maximum input voltage above which using HTS tapes is no longer beneficial, as the losses would exceed those of traditional copper tapes. As the output voltage is proportional to the input voltage, this limitation inherently sets a maximum achievable output voltage that can be reached by VIGs wound with HTS tapes.

It is relevant to compare the benefits of reduced ohmic losses with the benefits resulting from a reduced input switch inductance. To do so, the relative improvement obtained compared to the reference case of copper at 293 K is discussed for both changes in the inductances and in the losses. On the one hand, for a small number of turns, for example, focusing on the results for $N = 25$, the value of K_1 is improved by 11% when the inductance of the switch is reduced from 50 nH to 10 nH. In terms of ohmic losses, K_1 is improved by 3.8% for copper tapes at 77 K and by 5.4% for HTS tapes at 77 K with $i = 0.25$. On the other hand, for VIGs with long tape lengths, considering the results for $N = 200$, the relative improvement obtained with a better input switch inductance is 3.5% while the relative improvements resulting from reduced ohmic losses are 9% for copper at 77 K, and 13 % for HTS at 77 K with $i = 0.25$. First, these results show that for longer VIG lengths, reducing the ohmic losses is more effective than reducing the inductance of the input switch. Second,

these results show that HTS tapes, provided that they work in a regime with a small value of i, are able to provide a significant improvement of the voltage multiplication coefficient.

The theoretical predictions suggest a limitation around $i \simeq 0.25$. However, experimental measurements on the VIG SC-6-NF with a GTD switch at $u_0 \simeq 1$ kV show that the superconducting VIG still exhibited multiplication coefficients higher than those of the copper reference VIG at 77 K. In these experimental conditions, the VIG operated at $i \simeq 0.6$ as the VIG has a characteristic impedance $Z_0 \simeq 4.5\,\Omega$ corresponding to $I_{\max} \simeq 220$ A and the tape has an average critical current of $I_c \simeq 340$ A. This indicates that the updated model underestimates the output voltage, at least for the first peak. This is consistent with the observation made when comparing the updated model to experimental traces in Section 4.1.1, in which it was observed that the amplitude of the first peak predicted by the model was underestimated. Therefore, although AC losses will ultimately impose a limit on the current ratio i (and thus on u_0 and u_{out}), this limitation likely occurs at higher i values than predicted. This inherent limit of superconducting VIGs caused by losses underline that using HTS tapes in this topology of generators will benefit from the studies of how coated conductors behave under pulsed currents [38–41] as well as methods to reduce AC losses in coated conductors by filamentisation and striation [42–46].

5. Conclusions

In this paper, the use of superconducting materials was investigated to replace traditional copper tapes in Vector Inversion Generators to mitigate ohmic losses. The reason is that these losses play an important role in the limitation of the voltage multiplication efficiency of such generators when the total length of the generator is large, either with a large number of turns or a large inner diameter.

A first theoretical study shows that, in the presence of a copper stabilising layer, it is crucial to consider the magnetic diffusion of the current inside the layers of the HTS tape. The diffusion time required for the current density J to establish in the superconducting layer must be much smaller than the rise time of the pulse, which is dictated by the total length of the spiral. It shows that a certain length of conductors is required for superconducting VIGs to be efficient, meaning that superconducting VIGs are better for larger diameters and larger numbers of turns. This result is well aligned with the fact that ohmic losses are more pronounced for VIGs with a larger total length.

Another study was performed to show how an existing model of such generators can be updated to include the losses of HTS tapes in the resistance per unit length R' of VIGs, knowing an estimation of the nominal current in the conductor. The updated model was compared against experimental data, enabling predictions of the multiplication coefficient for larger diameters and an increasing number of turns. The results show that two parameters are of importance. First, the total length of the VIG should be large to benefit from reduced ohmic losses. Second, the limiting factor comes from the current ratio $i = I_{\max}/I_c$, which must be as low as possible to prevent the AC losses of the tapes from overcoming the benefits obtained by using

superconducting materials. Since reducing the temperature from 293 K to 77 K with a copper VIG already provides a non-negligible increase in the voltage multiplication efficiency, increased current ratios can render a copper VIG at cryogenic temperatures more efficient than a superconducting VIG. The current ratio i being directly related to the input voltage u_0, this sets a limit on the input voltage that can be used for superconducting VIGs, and, therefore also dictates a maximum output voltage that can be obtained.

Finally, experimental tests were performed with two types of HTS tapes: with and without a ferromagnetic substrate. Results show that it is important to choose an HTS tape without a ferromagnetic substrate because the losses caused by the ferromagnetic material counteract the intended benefit of using an HTS tape, resulting in lower multiplication coefficients than a similar VIG at room temperature wound with copper tapes.

Acknowledgment

This work was funded through the Win2Wal program financed by the *SPW-Recherche* department of the *Région Wallonne* (convention 2110062). We thank Dr. Mark Rikel for his help in obtaining the 40-mm wide coated conductor. Fruitful discussions with Prof. B. Vanderheyden are also acknowledged.

Appendix A. Semi-analytical model of the output voltage of a VIG

This section aims to provide a summary of the model we established in our previous work [7]. The model provides an expression of the normalised output voltage of vector inversion generators $B(p) = u_{\text{out}}/(2Nu_0)$ in the Laplace domain, in which p is the dimensionless Laplace variable. It is expressed as follows:

$$B(p) = \frac{-pF(p)}{p^2 + (1 - G(p))\,(\tau p + \omega_0^2)}. \tag{A.1}$$

In this expression, the functions $F(p)$ and $G(p)$ are expressed as:

$$F(p) = \frac{A(p) - P(p)}{1 - (p^4\tau_a^2 + 2p^3\tau_a\rho_a + p^2\rho_a)\,A(p)P(p)}, \tag{A.2}$$

$$G(p) = \frac{A(p) + P(p) + 2\left(p^2\tau_a + p\rho_a\right)A(p)P(p)}{1 - (p^4\tau_a^2 + 2p^3\tau_a\rho_a + p^2\rho_a)\,A(p)P(p)}. \tag{A.3}$$

These two expressions themselves contain the functions $A(p)$ and $P(p)$ which are expressed as:

$$A(p) = \left[p\sqrt{1 + \frac{\rho_0}{p}}\coth\left(\frac{p}{2}\sqrt{1 + \frac{\rho_0}{p}}\right) + p^2\tau_a + p\rho_a\right]^{-1}, \tag{A.4}$$

$$P(p) = \left[p\sqrt{1 + \frac{\rho_0}{p}}\coth\left(\frac{p}{2}\sqrt{1 + \frac{\rho_0}{p}}\right) + p^2\tau_p + p\rho_p\right]^{-1}. \tag{A.5}$$

This model is expressed by means of a set of dimensionless parameters that can be calculated based on the dimensions and the materials used to wind the VIG. Table A1 contains the list of the dimensionless parameters, as well as their mathematical expression and their physical meaning. In the expressions of the dimensionless parameters, different parameters related to the physics of VIG appear. Some are related to the input switch: L_{s} is the inductance of the switch and R_{s} is the resistance of the switch. Then, some are related to the waveguide aspect of VIGs: Z_0 is the lossless characteristic impedance of the waveguides, T is the time required for the electromagnetic wave to travel back and forth inside the spiral, and L', C' and R' are respectively the inductances, capacitances and resistances per unit length of the waveguides. Finally, some parameters are lumped RLC elements: L is the self inductance formed by the conductor wound in a spiral of N turns, C is the capacitance of the two conducting layers separated by dielectric layers, Z is the impedance of the load connected to the VIG, and L_{turn} and R_{turn} are respectively the inductance and resistance of the outer turn of the spiral.

In this paper, the parameters of interest are ρ_0 and ρ_{p}, which are functions of the resistance per unit length R' of the waveguides. These are the quantities that are affected by a change a conductivity, which is the purpose of replacing copper tapes with HTS coated conductors.

Parameter	Expression	Physical meaning
τ_{a}	$\frac{L_{\mathrm{s}}}{Z_0 T}$	Time constant associated with the "RL-like" circuit formed by the switch and the waveguide.
τ_{p}	$\frac{L_{\mathrm{s}}+L_{\mathrm{turn}}}{Z_0 T}$	Time constant associated with the "RL-like" circuit formed by the switch in series with the outer turn of the spiral and the waveguide.
ω_0	$\frac{T^2}{LC}$	Resonance frequency of the LC circuit formed by the vector inversion generators which acts simultaneously as a coil (conductor wound as a spiral) and a capacitor (two conducting layers separated by a dielectric layer).
τ	$\frac{T}{ZC}$	Load connected at the output of the VIG.
ρ_0	$\frac{R'T}{L'}$	Resistance of the waveguides.
ρ_{a}	$\frac{R_{\mathrm{s}}}{Z_0}$	Resistance of the switch.
ρ_{p}	$\frac{R_{\mathrm{s}}+R_{\mathrm{turn}}}{Z_0}$	Resistance of the switch in series with the outer turn of the spiral.

Table A1. Expression and physical meaning of all the dimensionless parameters appearing in the Laplace expressions of the semi-analytical model of the output voltage of vector inversion generators.

References

[1] Feng W, Rao P, Nimbalkar S, Chen Q, Cui J and Ouyang P 2023 *Materials* **16** 1693–1714
[2] Zhu B, Su H, Fang Z, Wu G and Wei X 2023 *Energies* **16** 2741–2754
[3] Ariztia L, Zhabin A, Lavrinovich I, de Ferron A S, Rivaletto M, Novac B M and Pecastaing L 2022 *IEEE Transactions on Plasma Science* **50** 3123–3130
[4] Kumar R, Novac B M, Sarkar P, Smith I R and Greenwood C 2008 300 kv tesla transformer based pulse forming line generator *IEEE International Power Modulators and High-Voltage Conference* pp 246–249
[5] Fitch R and Howell V 1964 *Proceedings of the Institution of Electrical Engineers* **111** 849
[6] Rühl F and Herziger G 1980 *Review of Scientific Instruments* **51** 1541–1547
[7] Wens T, Laurent P, Fagnard J F, Greffe C and Vanderbemden P 2023 *Journal of Applied Physics* **134** 094501
[8] Yan J, Parker S and Bland S 2021 *IEEE Trans. Power Electron.* **36** 10005–10019
[9] Shotts Z, Roberts Z and Rose M F 2009 Limits and failure modes in high voltage vector inversion generators *2009 IEEE Pulsed Power Conference* pp 902–907
[10] García-Tabarés L, Toral F, Munilla J, González L, Puig T and Obradors X 2025 *Rivista del Nuovo Cim.* Received 10 December 2024; Accepted 10 April 2025
[11] Nilsson E, Rivenc J, Rouquette J F, Tassisto M, Fallouh C, Ybanez L, Dönges S A, Weiss J, Radcliff K, van der Laan D, Gacnik D, Leferink J, Otten S, Dhallé M and ten Kate H J 2024 *IEEE Transactions on Applied Superconductivity* **34** 4801704
[12] Tixador P, Deleglise M, Badel A, Berger K, Bellin B, Vallier J C, Allais A and Bruzek C E 2008 *IEEE Transactions on Applied Superconductivity* **18** 774–778
[13] Ren L, Xu Y, Zuo W, Shi X, Jiao F, Liu Y, Deng J, Li J, Shi J, Wang S, Tang Y, Wen J, Han P, Qu Q, Liu H, Chen J, He Q, Jin T and Zhou S 2015 *IEEE Transactions on Applied Superconductivity* **25** 5701109
[14] Jiang Q, Majoros M, Hong Z, Campbell A M and Coombs T A 2006 *Superconductor Science and Technology* **19** 1164–1171
[15] Abrahamsen A B, Mijatovic N, Seiler E, Zirngibl T, Træholt C, Nørgård P B, Pedersen N F, Andersen N H and Østergård J 2010 *Superconductor Science and Technology* **23** 034019
[16] Chow C C, Ainslie M D and Chau K 2023 *Energy Reports* **9** 1124–1156
[17] Lee C, Son H, Won Y, Kim Y, Ryu C, Park M and Iwakuma M 2020 Progress of the first commercial project of high-temperature superconducting cables by kepco in korea *3rd International Conference on Electrical Materials and Power Equipment* (IEEE) pp 168–171
[18] Kinoshita Y, Yonenaka T, Ichiki Y, Akasaka T, Otabe E, Kiuchi M, Matsushita T, Hu N, Ni B and Ma T 2021 *Journal of Physics: Conference Series* **1975** 012037
[19] Song J B, Chaud X, Debray F, Paillot K, Fazilleau P, Lécrevisse T, Herrmannsdörfer T, Senatore C, Dhallé M and Smara A 2024 *IEEE Transactions on Applied Superconductivity* **34** Article 6600205, 5 pages
[20] van der Laan D C, Weiss J D and McRae D M 2019 *Superconductor Science and Technology* **32** 033001
[21] Liao H, Shchukin A, Parajuli R, Chaud X, Song J B, Zhang M and Yuan W 2024 *iEnergy* **3** 261–267
[22] Li X, Ainslie M, Song D, Yang W and Macián-Juan R 2025 *Superconductor Science and Technology* **38** 063001
[23] Norris W T 1970 *Journal of Physics D: Applied Physics* **3** 489
[24] Bobowski J S 2020 *arXiv* (*Preprint* 2011.00430)
[25] Hanlon J, Shotts Z, Rose M F and Best S 2007 High voltage solid state switched vector inversion generators *16th IEEE International Pulsed Power Conference* pp 918–922
[26] Kails K, Zhang H, Mueller M and Li Q 2020 *Superconductor Science and Technology* **33** 064006
[27] Jackson J D 1998 Magnetostatics, faraday's law, quasi-static fields *Classical Electrodynamics* (Wiley) 3rd ed
[28] Kraus J D and Fleisch D A 1999 *Electromagnetics: With Applications* 5th ed (WCB/McGraw-Hill)
[29] Simon N J, Drexler E S and Reed R P 1992 Properties of copper and copper alloys at cryogenic temperatures NIST Monograph 177 National Institute of Standards and Technology
[30] Lu J, Choi E S and Zhou H D 2008 *Journal of Applied Physics* **103** 064908
[31] Bae J H, Park H Y, Eom B Y, Seong K C and Baik S K 2010 *Physica C: Superconductivity and its Applications* **470** 1880–1882
[32] Kesgin I, Levin G A, Haugan T J and Selvamanickam V 2013 *Applied Physics Letters* **103** 252603

[33] Sundaram A, Zhang Y, Knoll A R, Abraimov D, Brownsey P, Kasahara M, Carota G M, Nakasaki R, Cameron J B and Schwab G 2016 *Superconductor Science and Technology* **29** 104007
[34] Cheetham P, Zhang Z, Kvitkovicova M, Wagner J, Kim C H, Graber L and Pamidi S V 2017 *IOP Conference Series: Materials Science and Engineering* **278** 012021
[35] Afif B, Oh S, Jeong M, Park J, Shin W, Jo U, Handito R, Park J, Kim G, Hahn G, Choi S, Hahn S and Kang H 2023 *IEEE Transactions on Applied Superconductivity* **33** 8001005
[36] Pal'chikov E I, Ryabchun A M and Krasnikov I Y 2012 *Technical Physics* **57** 292–301
[37] Rose M F, Shotts Z and Roberts Z 2005 High efficiency compact high voltage vector inversion generators *Proceedings of the 2005 IEEE Pulsed Power Conference*
[38] Tsuchiya Y, Sakai I, Mizuno K, Kohama Y, Yoshida Y and Awaji S 2023 *IEEE Transactions on Applied Superconductivity* **33** 8001105
[39] Tsuchiya Y, Mizuno K, Kohama Y, Zampa A, Okada T and Awaji S 2024 *IEEE Transactions on Applied Superconductivity* **34** 9500207
[40] Sirois F, Coulombe J, Roy F and Dutoit B 2010 *Superconductor Science and Technology* **23** 034018
[41] Bernstein P, McLoughlin C, Thimont Y, Sirois F and Coulombe J 2011 *Journal of Applied Physics* **109** 033915
[42] Grilli F and Kario A 2016 *Superconductor Science and Technology* **29** 083002
[43] Gömöry F, Solovyov M and Šouc J 2024 *IEEE Transactions on Applied Superconductivity* **34** 5901605
[44] Pekarčíková M, Frolek L, Necpal M, Cuninková E, Skarba M, Hulačová S, Ferenčík F and Bočáková B 2023 *Materials* **16** 7333
[45] Wulff A C, Abrahamsen A B and Insinga A R 2021 *Superconductor Science and Technology* **34** 053003
[46] Amemiya N, Enomoto N, Jiang Z, Kasai S, Saitoh T and Shiohara Y 2005 *Physica C* **426–431** 1267–1275